Journal of Polymer Research (2018) 25: 65
https://doi.org/10.1007/s10965-018-1471-0

ORIGINAL PAPER

Enhanced tensile strength and initial modulus of poly(vinyl alcohol) /graphene oxide composite fibers via blending poly(vinyl alcohol) with poly(vinyl alcohol)-grafted graphene oxide

Shengchang Zhang[1] · Pengqing Liu[1] · Xiangsen Zhao[1] · Jianjun Xu[1]

Received: 18 October 2017 / Accepted: 29 January 2018 / Published online: 6 February 2018

Abstract

Poly(vinyl alcohol)-grafted Graphene oxide (PVA-g-GO) as novel nanofillers were used to reinforce poly(vinyl alcohol) (PVA) composite fibers via simple wet spinning to promote homogeneous dispersion of reinforcing nanofillers as well as strengthen interfacial adhesion between nanofillers and matrix. Then the impact of these PVA chains grafted above GO sheets on the compatibility and dispersion of PVA-g-GO sheets in PVA fiber, the interfacial adhesion between nanofillers and matrix and the structure as well as property of PVA-g-GO/PVA fibers were studied systematically via characterizing morphology, aggregation structure and mechanical property of these composite fibers. These results showed that not only well dispersion and compatibility of PVA-g-GO sheets in composite fibers could be achieved, but also obvious enhancement in interfacial adhesion between nanofillers and matrix. Meanwhile, significant reinforcement in tensile strength and initial modulus of these composite fibers could also be obtained. Compared with neat PVA drawn fiber, tensile strength and initial modulus of these composite drawn fibers could increase by 39% and 69% with addition of 0.60 wt% of PVA-g-GO sheets, respectively. On the one hand, crystallization and orientation degree of these composite fibers could be improved because of the template-oriented effect of PVA-g-GO sheets during hot drawing. On the other hand, efficient load transfer between matrix and nanofillers in composite drawn fibers could be achieved easily because of the strong interfacial adhesion between nanofillers and matrix. These were also two main reasons for the obvious improvement in tensile strength and initial modulus of composite drawn fibers.

Keywords Functionalized graphene oxide · Poly(vinyl alcohol) fibers · Mechanical properties · Crystallization and orientation · Interfacial adhesion

Introduction

Recently, because of their unique structure and remarkable property at nanometer scale,carbon-based nanofillers had drawn an enormous amount of attention and opened a wide window of applications [1–6]. To date, many researchers had published that carbon-based nanofillers were suitable for reinforcing the mechanical property of polymeric fiber via mechanical blending because of their superior mechanical strength and prominent nanometer size effect [7–11]. For example, Poulin et al. [12] first prepared nanotube ribbons consisted of poly(vinyl alcohol) and single-walled carbon nanotubes (SWNTs), and the mechanical properties of obtained products could be enhanced obviously. Ruan et al. [13] found that the ultra strong polyethylene fibers with tensile strength of 4.2 GPa and strain at break of 5% could be produced via gel spinning with adding 5 wt% multi-walled carbon nanotubes. Chatterjee et al. [14] utilized graphene nanoplatelets (GnP) as reinforcing fillers to achieve the significant reinforcement in elastic modulus of polyamide 12 fibers from 600 MPa to 3200 MPa with adding 0.5 wt% GnP. Although the mechanical property of polymeric fiber could be improved obviously by blending carbon-based nanofillers, some obstacles were limiting their further application and development. On the one hand, when additions of carbon-based nanofillers were relatively high, they tended to aggregate

✉ Pengqing Liu
liupq@scu.edu.cn

[1] State Key Laboratory of Polymer Materials and Engineering, College of Polymer Science and Engineering, Sichuan University, Chengdu 610065, China

together in polymeric fibers because of the van der Waals' force among themselves. On the other hand, compound spinning fluids or melts would undergo lots of shearing, extrusion and high temperature during the fabrication processes of polymeric composite fibers, it would aggravate the aggregation of carbon-based nanofillers in composite fibers. The aggregation of nanofillers would not only reduce the interfacial adhesion between nanofillers and matrix as well as self-reinforcing effect in polymeric matrix, but also weaken the mechanical property of composite fibers as defects. How to further realize a homogeneous dispersion of nanofillers in the polymeric fibers and how to strengthen the interfacial adhesion between the nanofillers and matrix became two main challenges for researchers to achieve maximum reinforcement effect of nanofillers in polymeric fibers [15, 16].

Poly(vinyl alcohol) (PVA) as a conventional semicrystalline polymer exhibited not only outstanding biocompatibility and water solubility because of the existence of rich hydroxyl groups, but also excellent processability and non-toxicity [17, 18]. PVA fibers with high strength and modulus as reinforcement material had been widely used in national defense and military industry, construction industry and automobile industry, etc. [19, 20]. Introducing carbon-based nanofillers into PVA fiber was also a useful and practical method to further reinforce its mechanical property and broaden its applications. Graphene oxide (GO) sheets as a two-dimensional carbon material linked with abundant oxygen-containing functional groups would have much lower intermolecular van der Waals' force among them to keep their stable dispersion and individual exfoliation in polymeric matrix compared with pristine graphene sheets and have better compatibility with PVA matrix. Moreover, because of these intermolecular hydrogen bonding between oxygen-containing functional groups located at GO edges and hydroxyl groups linked to PVA matrix, the interfacial adhesion between GO sheets and PVA matrix would be stronger [21, 22]. Because of these, blending GO sheets into PVA fiber had more potential to achieve the reinforcement of the mechanical property of PVA composite fiber [23]. According to our previous study [24], the tensile strength and initial modulus of PVA composite fiber could be improved significantly with the addition of 0.1 wt% GO. However, the dispersion and exfoliation of GO sheets in composite fibers and the interfacial adhesion between GO sheets and PVA matrix would be depressed obviously when the addition of GO sheets increased to 0.5 wt%. Meanwhile, poor dispersion of GO sheets and weak interfacial adhesion between nanofillers and matrix would restrain the reinforcing effect of GO sheets. Lastly, the aggregated nanofillers would further deteriorate the mechanical property of the PVA composite fiber as impurities and defects. A further homogeneous dispersion and stable exfoliation of nanofillers at higher addition in PVA matrix would achieve if nanofillers would contain some PVA chains grafted on their surfaces to further depress the aggregation among nanofillers. At the same time, the compatibility between nanofillers and PVA matrix could be further increase due to the theory of similar dissolve mutually. Lastly, these PVA chains grafting above nanofillers could further enhance the interfacial adhesion between nanofillers and PVA fiber.

Taking these considerations into account, poly(vinyl alcohol) chains grafted graphene oxide sheets (PVA-g-GO) were prepared by in-situ polymerization and alcoholysis in our previous studies [25]. Moreover, we found that the mechanical properties of PVA-g-GO/PVA composite films could be improved obviously because of the efficient load transfer and the molecular-level dispersion of PVA-g-GO sheets in matrix. So these obtained PVA-g-GO sheets were expected to reinforce the mechanical properties of PVA composite fibers. In this paper, PVA-g-GO/PVA composite fibers would be prepared via mechanical blending PVA-g-GO sheets into PVA spinning solutions, after which the wet spinning method was conducted. The interfacial adhesion between nanofillers and composite fiber matrix, the dispersion as well as compatibility of nanofillers in these composite fibers, the morphology as well as aggregation structure of these composite fibers had been characterized systematically to investigate the impact of the PVA chains grafted above GO sheets on tensile strength and initial modulus of these composite fibers.

Experimental section

Materials

PVA with polymerization degree 1700 and hydrolysis 99%was obtained from SINOPEC Sichuan Vinylon Works (Chongqing, China). PVA-g-GO sheets were prepared via in-situ emulsion polymerization and alcoholysis reaction according to our previous studied [25], which contained about 24 wt% PVA chains measured by thermogravimetric analysis. α-Bromonaphthalene was provided by Best Chemical Reagent Company (Chengdu, China). Liquid paraffin, sodium sulfate (Na_2SO_4) and dimethyl sulfoxide (DMSO) were obtained by Kelong Chemical Reagent Company (Chengdu, China).

PVA-g-GO/PVA composite spinning solutions preparation

Firstly, PVA-g-GO sheets were dispersed in DMSO with stirring at 90 °C for 4 h. Furthermore, a further homogeneous dispersion of this mixture was achieved via ultrasonic dispersion at room temperature for 30 min. Meanwhile, an aqueous solution of 15 wt% PVA was obtained via dissolving specified mass PVA in distilled water with refluxing and stirring for 4 h at 98 °C. Finally, the prepared PVA-g-GO/DMSO dispersion

was quickly blended into the PVA aqueous solution keeping refluxing and rapid stirring at 98 °C for 90 min. A series of PVA-g-GO/PVA spinning solutions with different PVA-g-GO sheets addition were similarly fabricated. The formulations and sample codes for these spinning solutions were shown in Table 1.

The fabrication of PVA-g-GO/PVA composite fibers

A series of prepared composite spinning solutions were fabricated to composite as-spun fibers via wet spinning as shown in Scheme 1a. The coagulating bath consisted of the saturated Na_2SO_4 aqueous solution. Then, these as-spun fibers were drawn in hot air bath twice at 170 °C (first drawing) and 200 °C (second drawing). As for all as-spun fibers, the ratio of first drawing was 4.5 times, and the ratio of second drawing was 2 times. The total ratio of hot drawing was 9 times. Finally, treated PVA composite fibers were obtained after the process of heat setting at 220 °C as shown in Scheme 1b. Remarkably, according to our previous studies [25], the initial thermal decomposition temperature of the most of PVA chains grafted above GO was over 220 °C. So it could conclude that the pyrogenic decomposition of the most of PVA chains grafted above GO edges could not occur in the process of heat treatment.

Measurement and characterizations

The tensile strength and initial modulus of PVA-g-GO/PVA composite drawn fibers were characterized by an electronic fiber strength tester (Model: LLY-06, Laizhou Electron Instrument Company, Ltd., China). The stretch rate was 20 mm/min, and gauge length was 20 mm with a 10 cN load cell. And test temperature was 25 °C, test humidity is 65%.

A Nicolet Nexus-560 Fourier-transform infrared (FTIR) spectrometer was used to characterize the ATR (attenuated total reflectance)-FTIR spectra of these PVA-g-GO/PVA drawn fibers.

X-Ray diffraction measurements (XRD) (Model: X' Pert Pro, Philips Company, the Netherlands) was performed to observe the crystalline structure of these composite drawn fibers with Cu-Ka radiation (wavelength: 0.154 nm) at 40 kV.

Table 1 Sample code and formulations of PVA-g-GO/PVA spinning solution with different PVA-g-GO addition

Sample code	PVA/g	H_2O/g	PVA-g-GO/mg	DMSO/g
neat PVA	45	228	0	27
0.13 wt% PVA-g-GO/PVA	45	228	59	27
0.39 wt% PVA-g-GO/PVA	45	228	177	27
0.60 wt% PVA-g-GO/PVA	45	228	269	27

2D wide-angle X-Ray diffraction (2D–WAXD) (Model: D8 DISCOVER, Bruker Company, Germany) with Cu-Ka radiation (wavelength: 0.154 nm) was used to characterize the crystalline orientation of these composite drawn fibers at 40 kV (accelerating voltage). Hermans equation [26] as follow was used to calculate the crystalline orientation factor. And the data came from the angular width of the (101) meridional reflection.

$$f_c = \frac{3 < \cos^2\varphi > -1}{2} \qquad (2-1)$$

Where f_c was crystalline orientation factor, φ was the angle between molecular chain axis and fiber axis, and the average denoted by the angle bracket was calculated as follow [27]:

$$< \cos^2\varphi > = \frac{\int_0^{\frac{\pi}{2}} I(\varnothing)\sin\varnothing\cos^2\varnothing d\varnothing}{\int_0^{\frac{\pi}{2}} I(\varnothing)\sin\varnothing d\varnothing} \qquad (2-2)$$

Where I(∅) was the X-Ray intensity of the resolved peak at azimuthal angle ∅.

Transmission electron microscopy (TEM) (Model: JEM-2100F, Japan Electron Optics Laboratory Company, ltd., Japan) with an accelerating voltage of 200 kV was used to observe the morphology of neat GO sheets and PVA-g-GO sheets. At the same time, the cross-sectional images of these composite as-spun fibers would also be observed by TEM. Ultrathin sections microtomed of composite as-spun fibers were obtained via using an ultratome (Model: MT-6000, DuPont Company, the USA) at liquid nitrogen. Finally, neat GO sheets, PVA-g-GO sheets and ultrathin sections were observed above copper grid.

In order to investigate the dispersion and compatibility of nanofillers in PVA matrix, composite as-spun fibers were broken off at liquid nitrogen before observation. The cross-sectional morphology of these composite as-spun fibers were observed by scanning electron micrographs (SEM) (Model: JSM-5900LV, JEOL, Japan) with 20 KV accelerating voltage. And these cross-sections of composite as-spun fibers and composite drawn fibers obtained after tensile fracture were also observed by SEM to study the interfacial adhesion between PVA-g-GO sheets and PVA matrix.

Dynamic mechanical analysis (DMA) (Model: Q800, TA Company, the USA) was used to characterize loss tangent (tan δ) and loss modulus of these composite as-spun fibers and composite drawn fibers under constant temperature and humidity (temperature: 25 °C, relative humidity: 65%). The fibrous samples were tested under stretching mode from 25 to 110 °C with a heating rate of 3 °C/min and a frequency of 3.5 Hz.

Overall chains orientation structure of these composite drawn fibers were characterized by birefringence method using immersion method (also called Beck line method) via polarizing microscope. The values of birefringence (Δn) of

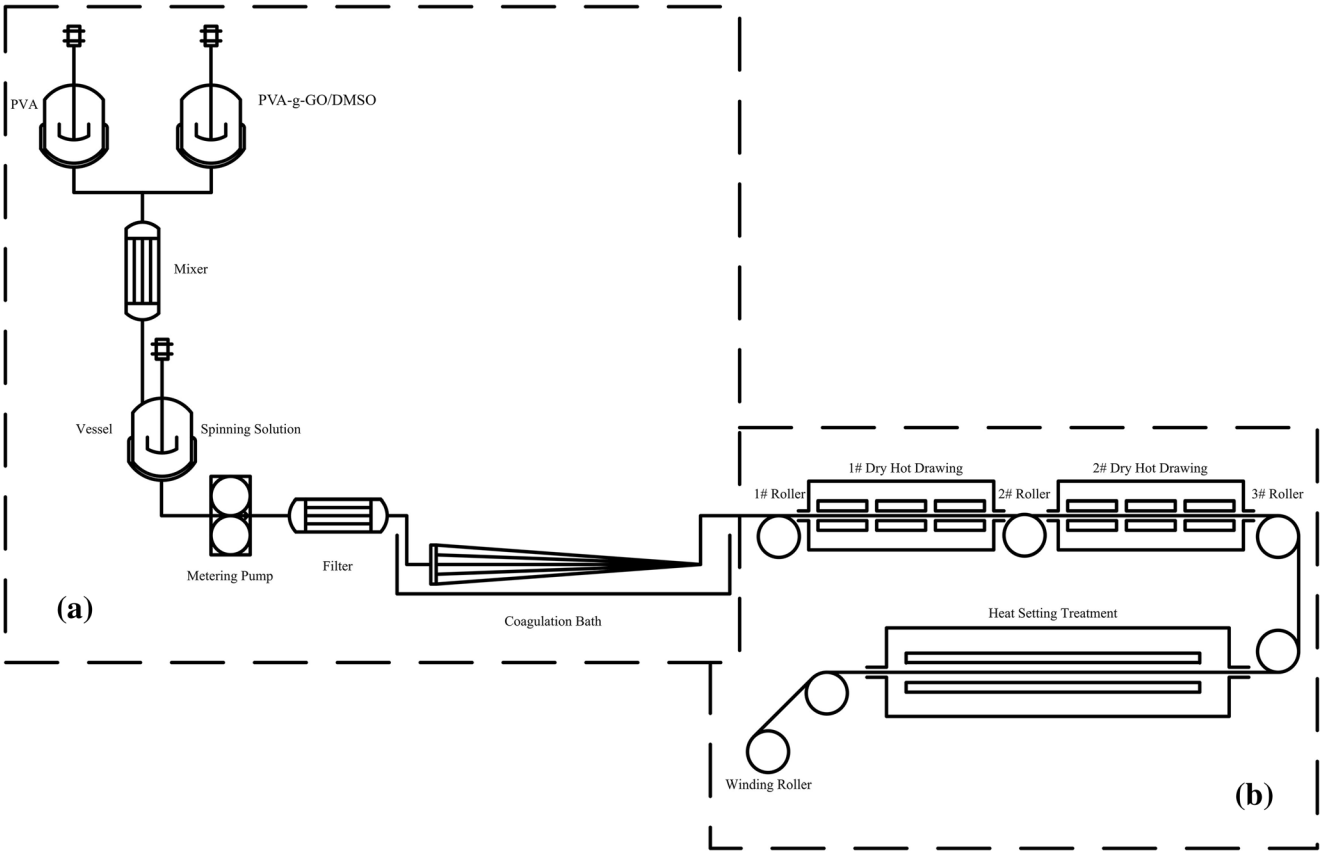

Scheme 1 Schematic diagram of (**a**) wet spinning of composite spinning solution and (**b**) heat treatment of composite as-spun fiber

these composite drawn fibers were equal to the difference between their parallel refractive indices ($n_{\parallel}$) and their perpendicular refractive indices ($n_{\perp}$). A series of immersion solutions were consisted of α-bromonaphthalene and atolein, and the mass fraction of α-bromonaphthalene increased from 0 wt% to 100 wt%.

Differential scanning calorimetry (DSC) (Model: DSC 204F1, Netzsch Instruments Inc., Germany) was used to measure the crystallization degree and the value of melting peak of these composite drawn fibers. The test was done under a temperature range from 10 to 240 °C with a linear heating rate of 10 °C/min. The crystallization degree of these composite drawn fibers was calculated from the ratio $\Delta H_m/\Delta H_0$, ΔH_m was the measured melting enthalpy and ΔH_0 was the enthalpy of neat PVA crystal (138.6 J/g) [24].

Results and discussions

Dispersion and morphology of nanofillers into as-spun fibers

Firstly, the morphology of neat GO sheets and PVA-g-GO sheets were observed via TEM. As shown in Fig. 1a, b, the morphology of neat GO sheets was clean, transparent and flake-like. However, when PVA chains were grafted on the surface of GO sheets, the morphology of modified GO sheets had changed. As shown in Fig. 1c, d, e and f, some dark spots and binding (circled by red dotted line) were observed on the surface of GO sheets. According to previous literatures [28, 29], it was attributed to the some PVA chains grafted on the surface of GO sheets. After drying, the grafted PVA chains collapsed above the surface of GO sheets to form nanosized domains that related to the dark spots observed. Secondly, the size of neat GO sheet and PVA-g-GO sheet were also obtained via TEM images. As shown in Fig. 1b and f, the size of PVA-g-GO sheet would no change obviously after modification compared with neat GO sheet. The length or width of both neat GO sheet and PVA-g-GO sheet was about 200–400 nm.

The dispersion and compatibility of PVA-g-GO sheets in PVA-g-GO/PVA as-spun fibers were characterized via SEM. The images of cross-sectional morphology of neat PVA as-spun fiber and these composite as-spun fibers were shown in Fig. 2. Compared with neat PVA as-spun fiber, the cross-sectional morphology of these composite as-spun fibers with increasing addition of PVA-g-GO sheets (from 0.13 wt% to 0.60 wt%) were still smooth, compact and homogeneous as neat PVA as-spun fiber. It could indicate that not only the compatibility of PVA-g-GO sheets with PVA matrix was very well with different PVA-g-GO sheets loadings in composite

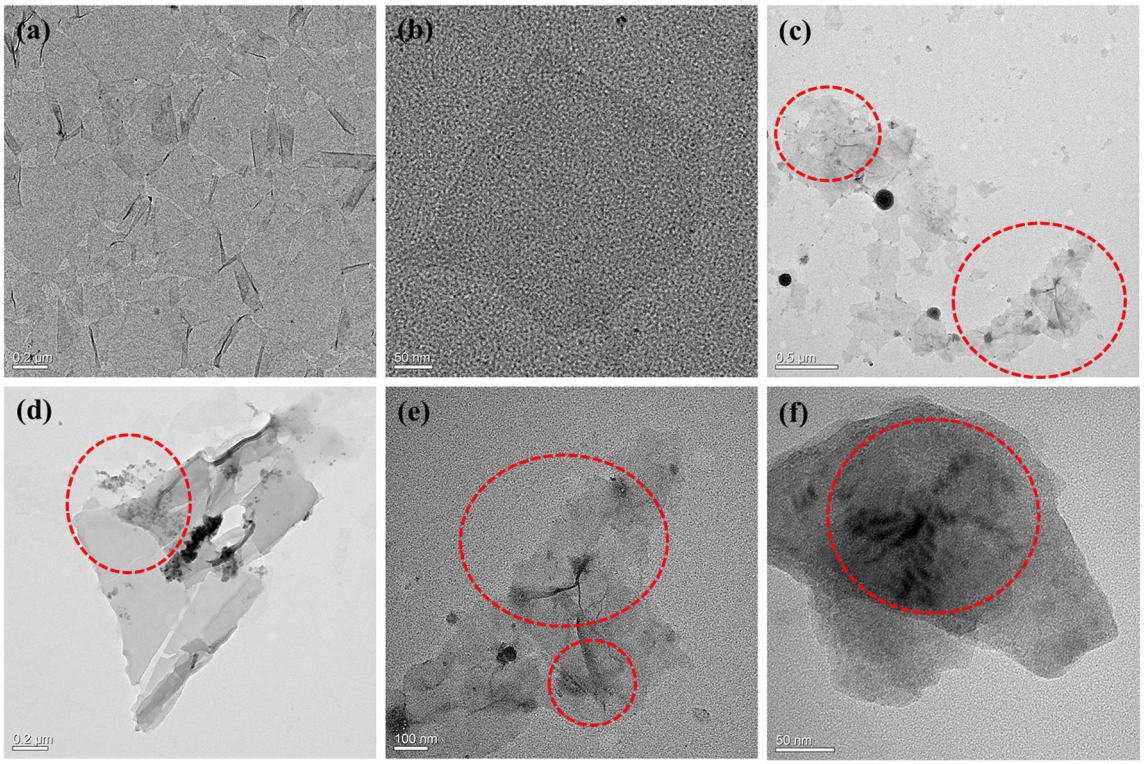

Fig. 1 TEM images of the morphology of (**a**) and (**b**) neat GO sheets (**c**–**f**) PVA-g-GO sheets

as-spun fibers, but also the molecular-level dispersion of PVA-g-GO sheets could be achieved. Meanwhile, the well compatibility and molecular-level dispersion of PVA-g-GO sheets could not deteriorate with increasing nanofillers loadings. It was crucial to realize the maximum reinforcement effect of PVA-g-GO sheets in composite fibers at higher loading level.

TEM images of the cross-sectional ultrathin section of PVA-g-GO/PVA as-spun fibers as shown in Fig. 3 were observed to analyze the morphology and size dimension of PVA-g-GO sheets in these composite as-spun fibers and further ensure the dispersion and exfoliation of these nanofillers. The thickness of PVA-g-GO sheets in PVA fiber matrix was about 3–10 nm and the length or width of these nanofillers

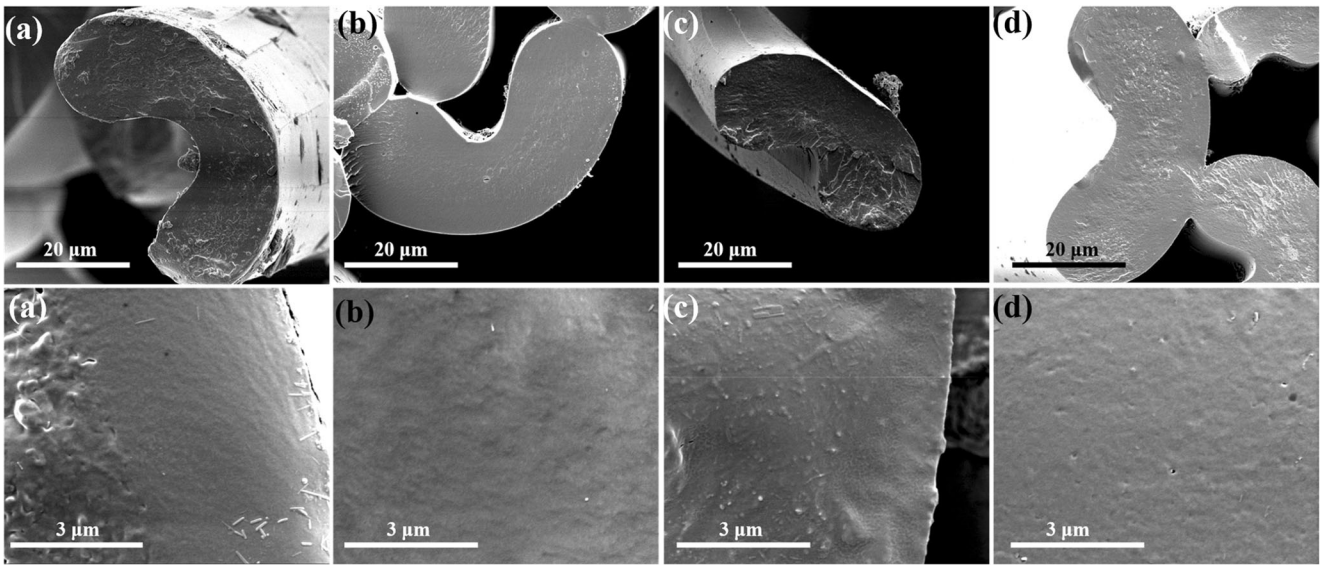

Fig. 2 The cross-sectional images of neat PVA and PVA-g-GO/PVA as-spun fibers: (**a**) neat PVA (**b**) 0.13 wt% PVA-g-GO/PVA (**c**) 0.39 wt% PVA-g-GO/PVA (**d**) 0.60 wt% PVA-g-GO/PVA (magnification of the first row: 5,000X; magnification of the second row: 40,000X)

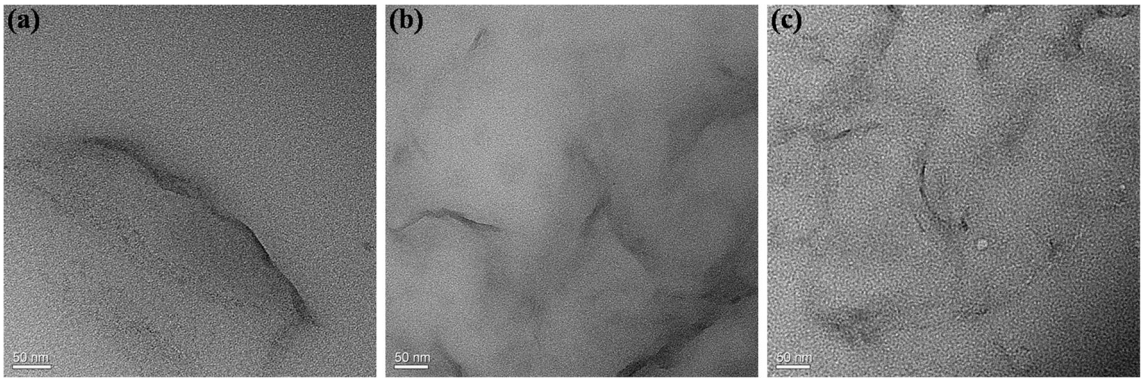

Fig. 3 TEM images of ultrathin section of cross-sectional of PVA-g-GO/PVA as-spun fibers (**a**) 0.13 wt% PVA-g-GO/PVA (**b**) 0.39 wt% PVA-g-GO/PVA (**c**) 0.60 wt% PVA-g-GO/PVA

was about 150–400 nm with different PVA-g-GO loadings (from 0.13 wt% to 0.60 wt%). According to the results from TEM images of PVA-g-GO sheet (Fig. 1f), the length or width of nanofillers in PVA matrix did not change obviously. It indicated that the dispersion of these nanofillers in composite as-spun fibers could keep homogeneous and would not deteriorate with increasing addition of these nanofillers. Meanwhile, most of nanofillers in composite as-spun fibers were exfoliated as individual sheet, only a few PVA-g-GO sheets were dispersed in composite as-spun fibers as 2–3 layers stacked sheets. There were two main reasons for these phenomenon and results. On the one hand, the intermolecular van der Waals' force among nanofillers which would lead to the obvious aggregation among them would be greatly weaken because of these PVA chains grafted above GO sheets. Furthermore, these PVA chains could also further promote the individual exfoliation of PVA-g-GO sheets. On the other hand, these PVA chains grafted above GO sheets was chemically similar to PVA fiber matrix. Because of the theory of similar dissolve mutually, they could also promote the compatibility between nanofillers and composite as-spun fiber matrix and further keep uniform dispersion and individual exfoliation of these nanofillers in composite as-spun fibers.

Interfacial adhesion between nanofillers and fiber matrix

The strong interfacial adhesion between nanofillers and polymeric fiber matrix was necessary and important to achieve the reinforcing effect of nanofillers. So the cross-sectional morphology of neat PVA and PVA-g-GO/PVA fibers obtained after tensile fracture were observed via SEM to study these strong interfacial adhesions. As shown in Fig. 4A and B, the cross-sectional morphology of PVA-g-GO/PVA fibers would become coarser and rougher compared with neat PVA fiber not only in as-spun but also in drawn fibers. These changes in microstructure features of composite fibers after adding PVA-g-GO sheets was attributed to the intermolecular entanglements between PVA-g-GO sheets and PVA matrix, evincing strong interfacial adhesion between nanofillers and polymeric matrix. It was because that these PVA chains bonded above PVA-g-GO sheets would form intermolecular interactions with those PVA matrix chains thus forming intermolecular entanglements. At the same time, some microfibrous structure (circled by red line) appeared on the surface of cross section after adding PVA-g-GO sheets in drawn fibers. It was also attributed to the existence of interfacial adhesion between PVA-g-GO sheets and PVA matrix in composite drawn fibers. Remarkblely, the roughness of cross section and the amount of microfibrous structure could be further improved with increasing the addition of PVA-g-GO sheets. From these results, it could conclude that there were strong interfacial adhesions between PVA-g-GO sheets and PVA fibers matrix in both as-spun and drawn fibers. And these interfacial adhesions would be strengthened gradually with increasing PVA-g-GO sheets addition.

Additional evidence for the existence of the interfacial adhesion between PVA-g-GO sheets and PVA fibers matrix came from DMA as shown in Fig. 5. As for PVA-g-GO/PVA as-spun fibers, it could be found that the loss modulus and the peak values of tan δ of these composite as-spun fibers were both increased compared with neat PVA as-spun fiber as shown in Fig. 5a and b. These observations could be attributed to the improved PVA-g-GO sheets dispersion in the PVA matrix and enhanced interfacial adhesion between these nanofillers and composite as-spun fiber matrix [30, 31]. On the one hand, the PVA chains grafted above nanofillers could form strong intermolecular entanglements with PVA matrix chains. These enhanced intermolecular entanglements would improve the efficiency of load transfer from composite as-spun fiber matrix to nanofillers, resulting in an increase in loss modulus because of more energy loss and dissipation in PVA-g-GO/PVA as-spun fibers with tensile and elevated temperatures [32, 33]. On the other hand, these intermolecular entanglements and adhesion would also reduce the mobility of PVA matrix chains around the PVA-g-GO sheets. With the effectively discouraging the movement of PVA matrix chains, the glass transition temperatures (tan δ peak values) of PVA-g-

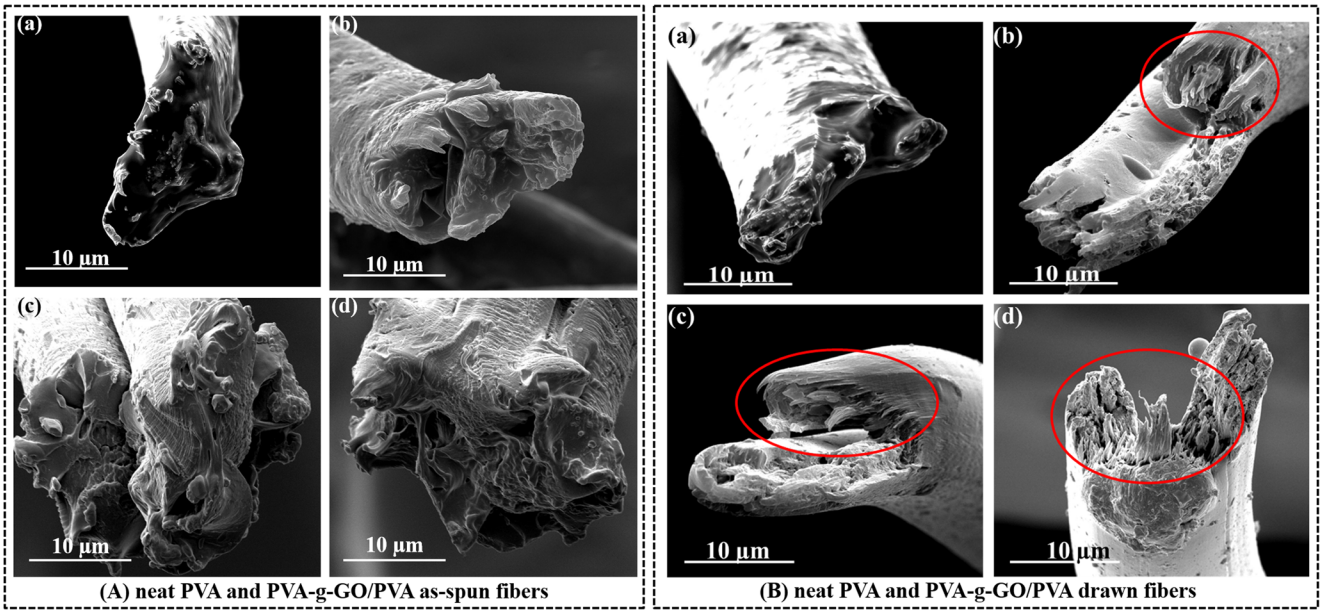

Fig. 4 SEM images of cross-sectional morphology of (**A**) neat PVA and PVA-g-GO/PVA as-spun fibers (**B**) neat PVA and PVA-g-GO/PVA drawn fibers: (a) neat PVA (b) 0.13 wt% PVA-g-GO/PVA (c) 0.39 wt% PVA-g-GO/PVA as-spun fibers (d) 0.60 wt% PVA-g-GO/PVA (magnification: 10,000X)

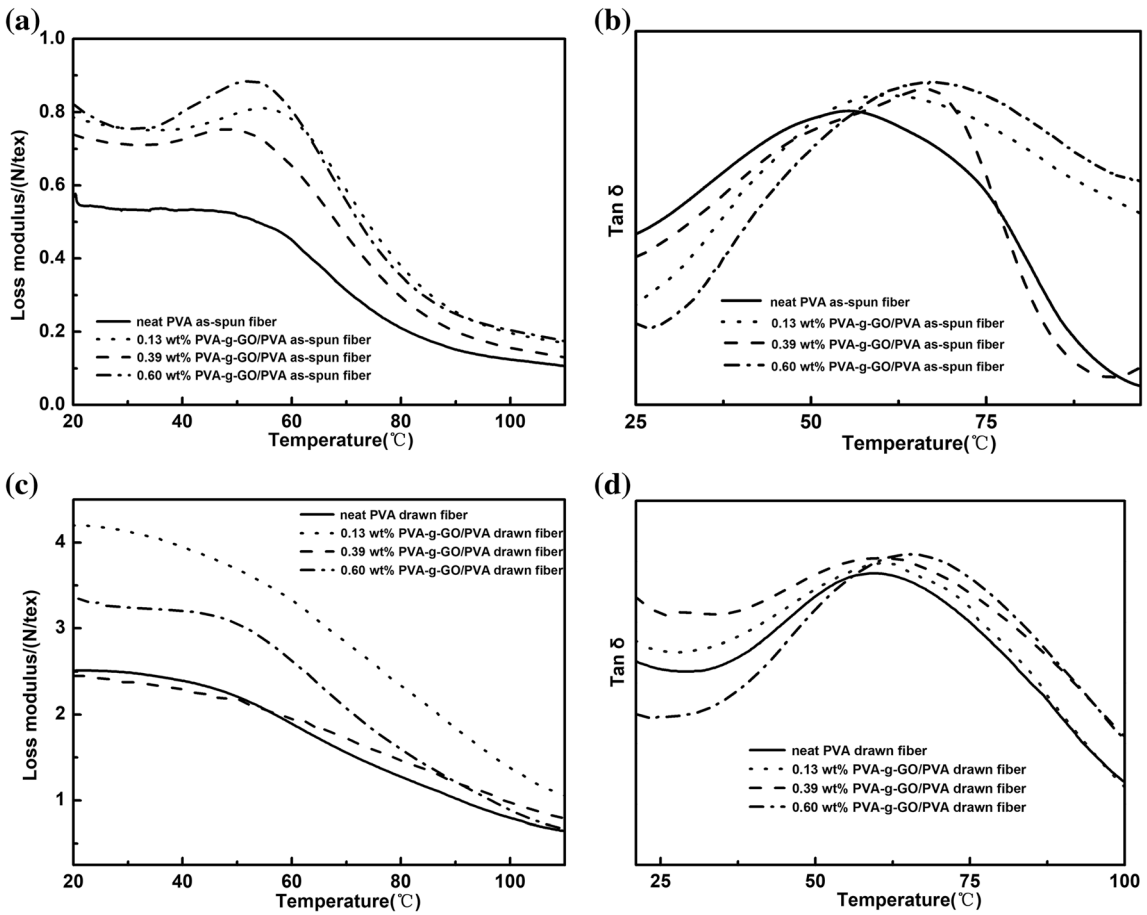

Fig. 5 DMA results of (**a**) loss modulus of PVA-g-GO/PVA as-spun fibers (**b**) tan δ of PVA-g-GO/PVA as-spun fibers (**c**) loss modulus of PVA-g-GO/PVA drawn fibers (**d**) tan δ of PVA-g-GO/PVA drawn fibers

GO/PVA as-spun fibers would be increased [34, 35]. So these results confirmed that the strong interfacial adhesion between these nanofillers and PVA matrix existed in these composite as-spun fibers. Not only composite as-spun fibers, the loss modulus and the peak values of tan δ of these composite drawn fibers were also both increased compared with neat PVA drawn fiber as shown in Fig. 5c and d. It could also confirm that these interfacial entanglements and adhesion would still exist in composite drawn fiber after the process of heat treatment. Remarkably, the pyrogenic decomposition of the most of PVA chains grafted above these nanofillers could not occur during the heat treatment process of as-spun fibers. So this strong interfacial adhesion between nanofillers and polymeric matrix in these composite drawn fibers could also still exist via the intermolecular entanglements between these grafted PVA chains and those PVA matrix chains.

To further ensure the existence of interfacial adhesion between these nanofillers and polymeric matrix in composite drawn fibers, ATR-FTIR spectra was employed to investigate it. As shown in Fig. 6, these wavenumber changes of -OH stretching vibration of PVA fiber matrix (around 3300 cm^{-1}) were closely related to intermolecular interactions between nanofillers and the polymeric matrix. It could be found that the wavenumber of -OH stretching vibration peak value shifted gradually to a lower position with increasing of PVA-g-GO sheets loadings. This phenomenon also indicated that the interfacial adhesion between nanofillers and polymeric matrix in composite drawn fibers would gradually strengthen because of these strong intermolecular entanglements and interactions between grafted PVA chains and PVA matrix chains in composite drawn fibers [36].

Orientation structure of composite drawn fibers

Generally speaking, the mechanical property of polymeric fibers was closely related to their orientation and crystallization structures [37, 38]. Furthermore, the orientation behavior of polymeric matrix chains during the process of hot drawing would further promote the crystallization process of polymeric as-spun fiber. To investigate the impacts of PVA chains grafted above PVA-g-GO sheets on the overall chains orientation structure of PVA-g-GO/PVA composite fibers during hot drawing, birefringence method was utilized. The birefringence values of neat PVA and PVA-g-GO/PVA drawn fibers were shown in Table 2. As well known, the birefringence value of polymeric fiber was positively linear-correlated to their overall chains orientation degree. So according to these data from Table 2, it could found that the overall PVA matrix chains orientation degree of these composite drawn fibers would be improved gradually via increasing PVA-g-GO sheets loadings.

Overall chains orientation degree of polymeric fibers included amorphous orientation degree and crystalline orientation degree. To further make sure whether PVA-g-GO sheets could improve the crystalline orientation or amorphous orientation of composite fibers, 2D–WAXD was used to investigate these changes of crystalline orientation structure of these composite drawn fibers. No matter neat PVA drawn fiber or PVA-g-GO/PVA drawn fibers, their diffraction spots which represented their crystalline orientation degree were bright and concentrated as shown in Fig. 7. It indicated that all drawn fibers would have very highly ordered crystals with extensive crystal orientation. Moreover, compared with neat PVA drawn fiber,

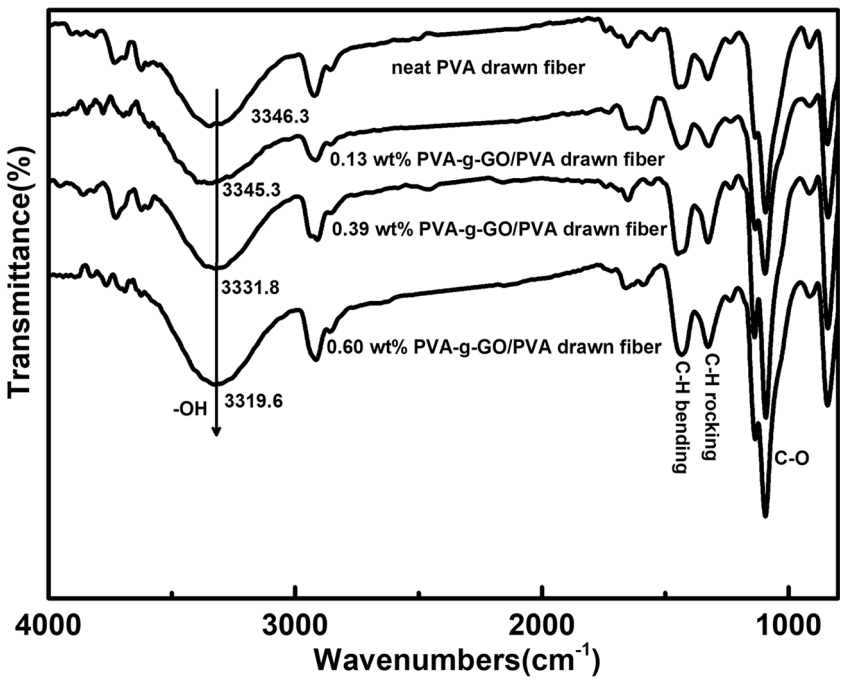

Fig. 6 ATR-FTIR spectra of neat PVA and PVA-g-GO/PVA drawn fibers with same draw ratio

Table 2 The birefringence (Δn) of PVA-g-GO/PVA drawn fibers with same draw ratio

Sample	$n_{\parallel}$	$n_{\perp}$	$\Delta n \times 10^3$
neat PVA	1.5608	1.5176	43.2
0.13 wt% PVA-g-GO/PVA	1.5534	1.5092	44.2
0.39 wt% PVA-g-GO/PVA	1.5534	1.5092	44.2
0.60 wt% PVA-g-GO/PVA	1.5582	1.5131	45.1

Table 3 The crystalline orientation factor of PVA-g-GO/PVA drawn fibers with same draw ratio

Sample	Crystalline orientation factor
neat PVA drawn fiber	0.932
0.13 wt% PVA-g-GO/PVA drawn fiber	0.935
0.39 wt% PVA-g-GO/PVA drawn fiber	0.942
0.60 wt% PVA-g-GO/PVA drawn fiber	0.943

the diffraction bright spot areas of these composite drawn fibers decreased gradually with increasing nanofillers loadings. It could conclude that the crystalline orientation factors of these composite drawn fibers could be further increased gradually during the process of hot drawing with increasing these nanofillers loadings [24]. Lastly, the crystalline orientation factor values of these drawn fibers were listed in Table 3.

Apart from crystalline orientation, the mechanical property of polymeric fiber was also closely related to its amorphous orientation [39]. As for the amorphous orientation factor of PVA-g-GO/PVA drawn fibers, it was hard to measure them directly. So these changes of amorphous orientation structure of PVA-g-GO/PVA drawn fibers during hot drawing were speculated indirectly via combining these results from birefringence method and 2D–WAXD. We could found that the improving of overall molecular chains orientation degree and crystalline orientation factor of these drawn fibers after adding PVA-g-GO sheets during hot drawing were relatively low. And according to comparing the improving extent of the two, it could conclude that the change of overall chains orientation degree was mainly determined by the change of crystalline orientation degree. So we speculated that the change of amorphous orientation structure of these drawn fibers after adding PVA-g-GO sheets during hot drawing was not obvious.

These orientation structure changes of these composite drawn fibers after adding PVA-g-GO sheets were closely related with these intermolecular entanglements between grafted PVA chains and PVA matrix chains. As shown in Scheme 2, these intermolecular entanglements and interfacial adhesion between PVA-g-GO sheets and PVA matrix could be

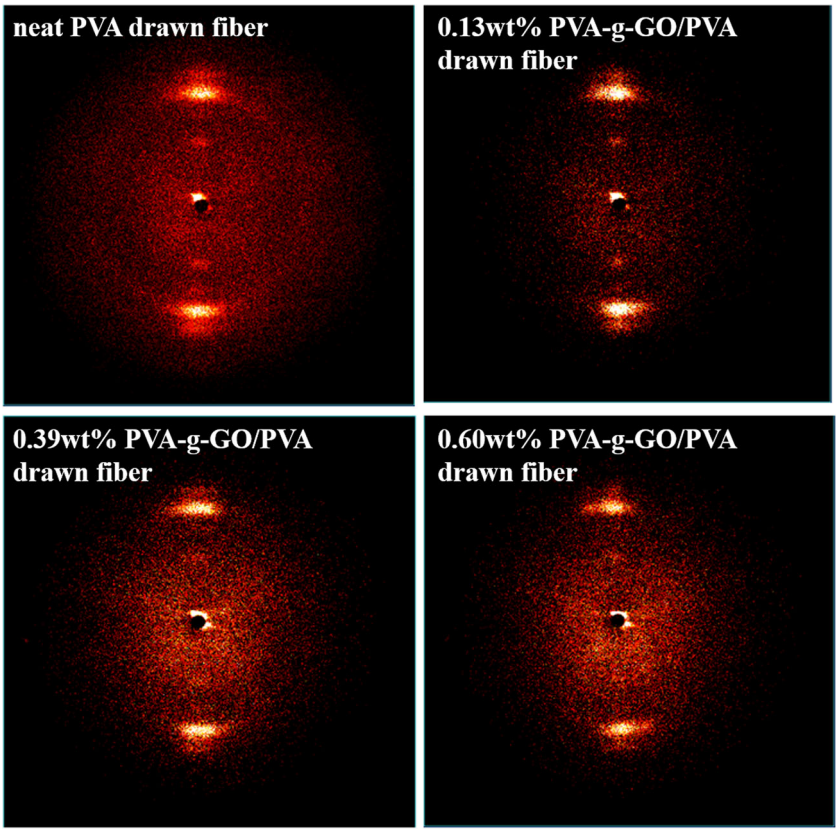

Fig. 7 2D-WAXD images of PVA-g-GO/PVA drawn fibers with same draw ratio

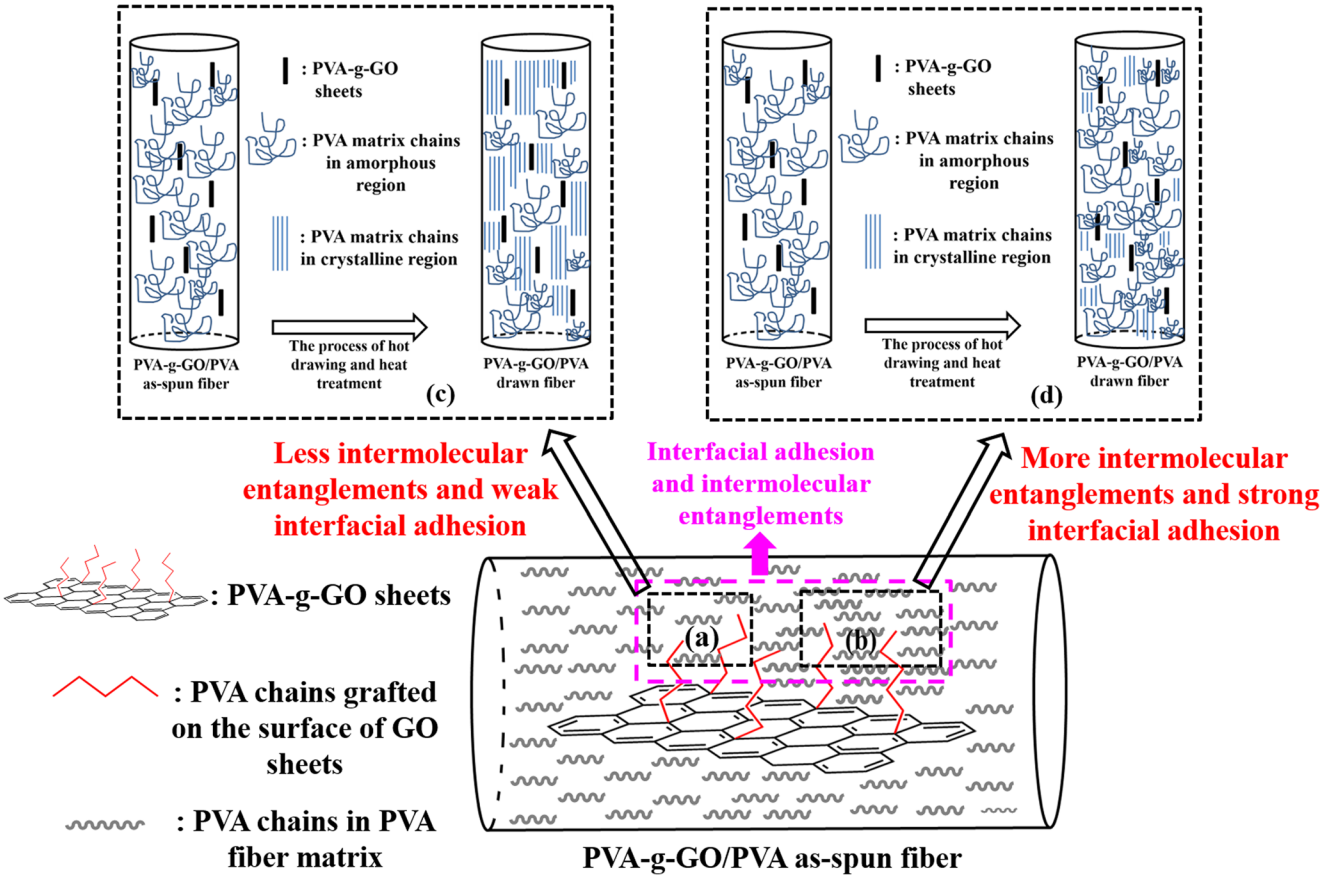

Scheme 2 Proposed structural model of intermolecular adhesion between PVA-g-GO sheets and PVA matrix in as-spun fibers: (**a**) less intermolecular entanglements (**b**) more intermolecular entanglements; and their related model before and after hot drawing: (**c**) less intermolecular entanglements and (**d**) more intermolecular entanglements

divided into two kind situations: (a) the interfacial adhesion and intermolecular entanglements were relatively weak; (b) the interfacial adhesion and intermolecular entanglements were relatively strong. When these intermolecular entanglements and interfacial adhesion were relatively weak as shown in Scheme 2a, the mobility of PVA matrix chains around these naofillers was relatively well. PVA-g-GO sheets could further promote the ordered and tight arrangement of PVA matrix chains via self template-oriented effect [24, 40, 41] during the process of hot drawing as shown in Scheme 2c. It helped to realize the improving of the overall chains orientation degree and crystalline orientation degree of PVA-g-GO/PVA composite drawn fibers. However, when these intermolecular entanglements and interfacial adhesion were relatively strong as shown in Scheme 2b, the mobility of PVA matrix chains around PVA-g-GO sheets and their extension and arrangement along the direction of tensile stress during hot drawing would be limited obviously because of these strong entanglements and adhesion. So the template-oriented effect of these nanofillers was difficult to play during the process of hot drawing, and further tight and ordered arrangement of PVA matrix chains around PVA-g-GO sheets during hot drawing were difficult to achieve. Furthermore, because of these strong intermolecular entanglements and adhesion between PVA-g-GO sheets and PVA matrix, the arrangement of most of PVA matrix chains around PVA-g-GO sheets was still disordered after hot drawing as shown in Scheme 2d [25, 42]. That was not only the reason why these changes of amorphous orientation structure were not obvious, but also the reason why the improving of overall and crystalline chains orientation factor of these drawn fibers were relatively low.

Crystalline structure of composite drawn fibers

Firstly, XRD intensity curves were used to investigate these changes of the crystalline structure and crystallization degree of these composite drawn fibers with increasing PVA-g-GO sheets loadings. As shown in Fig. 8, the diffraction peaks at 2θ of 11.4 °, 19.6 ° and 22.5 ° corresponded to the crystalline diffraction peaks of neat PVA drawn fiber [43]. These characteristic crystalline diffraction peaks of PVA-g-GO/PVA composite fibers were similar to neat PVA drawn fibers with increasing these nanofillers

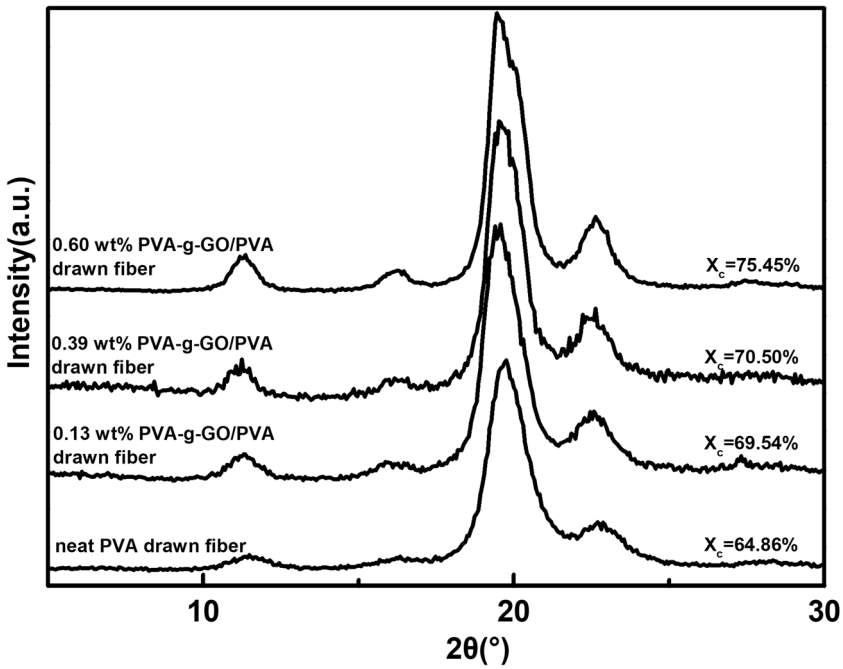

Fig. 8 XRD intensity curves of the PVA-g-GO/PVA composite fibers with same draw ratio

loadings. These results indicated that the crystalline structures of these composite drawn fibers would not change after introducing PVA-g-GO sheets. Meanwhile, it could find that the area and intensity of these crystalline diffraction peaks of these composite drawn fibers would increase gradually along with increasing the addition of these nanofillers. It indicated that the crystallization degree of these composite drawn fibers would increase gradually with increasing PVA-g-GO sheets loadings. The crystalline data calculated via MDI Jade 6.0 software indicated that the crystallization degree of 0.60 wt% PVA-g-GO/PVA composite fiber could increase by about 10% compared with neat PVA drawn fiber, all these results were listed in Fig. 8.

To further characterize and ensure the improvement in crystallization degree of these composite drawn fibers after adding PVA-g-GO sheets, DSC curves and data from the first heating process of all drawn fibers were analyzed. Compared with neat PVA drawn fiber, the crystallization degrees of these composite drawn fibers were gradually increased with increasing PVA-g-GO sheets loadings as shown in Fig. 9. The increasing of crystallization degree of PVA-g-GO/PVA

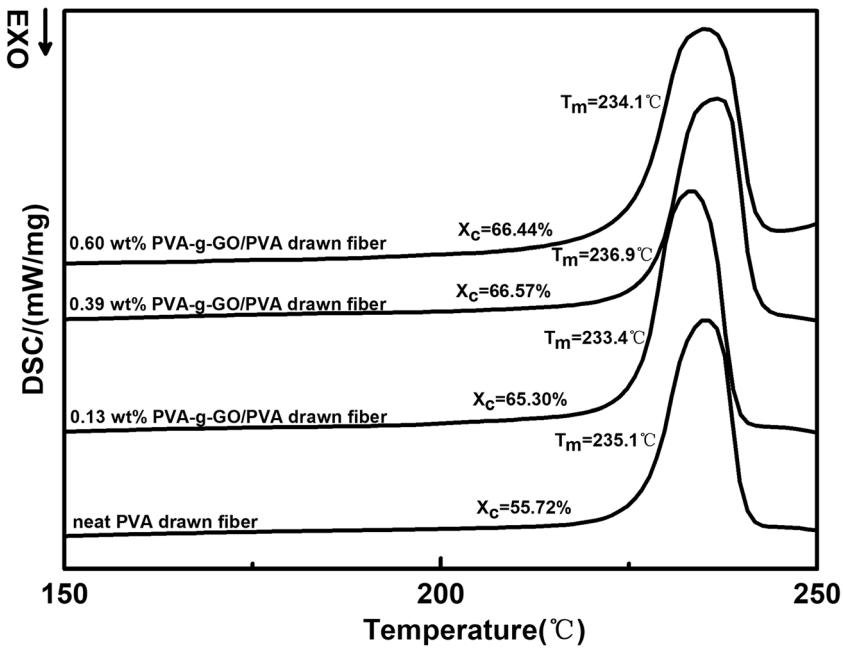

Fig. 9 DSC curves of PVA-g-GO/PVA composite fibers with same draw ratio

composite fibers was closely related to the increasing of overall and crystalline chains orientation degree of these composite drawn fibers during the process of hot drawing. The ordered and compact arrangement of PVA matrix chains during hot drawing could further promote the crystallization process of PVA matrix chains.

As for these changes of melting peak value of PVA-g-GO/PVA drawn fibers, on the one hand, it was attributed to the crystalline structure of PVA-g-GO/PVA drawn fibers. On the other hand, it was also closely related with the ordered arrangement of PVA matrix chains. When these intermolecular entanglements between PVA-g-GO sheets and PVA matrix were relatively weak, the ordered arrangement and induced crystallization of PVA matrix chains during hot drawing could be achieved because of the template-oriented effect of PVA-g-GO sheets, resulting in an increase in melting peak value of PVA-g-GO/PVA drawn fibers. However, when these intermolecular entanglements were relatively strong, the ordered arrangement of PVA matrix chains around PVA-g-GO sheets would be damaged, and the crystallization process of PVA matrix chains during hot drawing would also be limited, resulting in a decrease in melting peak value of these composite drawn fibers. So these changes of melting peak value of these composite drawn fibers with different nanofillers loadings were irregular as shown in Fig. 9.

Mechanical properties of PVA-g-GO/PVA composite fibers

The tensile strength and initial modulus of these composite drawn fibers and neat PVA drawn fiber were listed in Table 4, and the tensile stress-strain behaviors of these composite drawn fibers and neat PVA drawn fiber were shown in Fig. 10. Compared with neat PVA drawn fiber, the tensile strength and initial modulus of these composite drawn fibers would increase obviously with increasing PVA-g-GO sheets loadings. With 0.60 wt% PVA-g-GO sheets incorporated, the tensile strength of composite drawn fiber increased by 39% from 0.906 GPa to 1.257 GPa, while Young's modulus was raised by 69% from 15.690 GPa to 26.439 GPa. Compared with neat PVA drawn fiber, the strain after breakage of these composite drawn fibers would gradually reduce with increasing nanofillers loadings.

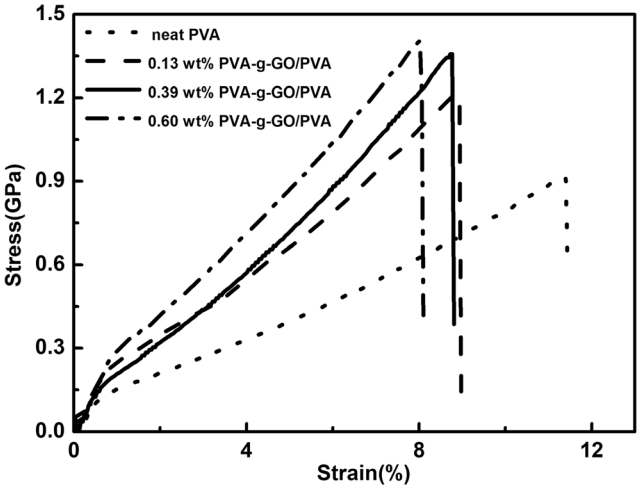

Fig. 10 Representative stress-strain behavior for PVA-g-GO/PVA drawn fibers with different PVA-g-GO sheets loadings

There were two main reasons for the obvious improvement in tensile strength and initial modulus of PVA-g-GO/PVA drawn fibers. On the one hand, it was attributed to the increasing of crystallization degree and crystalline orientation degree of these composite drawn fibers during the process of hot drawing after adding PVA-g-GO sheets. It helped to minimize stress focus and reduce molecular structure defects. Furthermore, it also helped to improve the strength and modulus of PVA matrix chains and increase the probability of fragmentation of PVA matrix chains during the process of tensile fracture. On the other hand, it was closely related to these high intermolecular entanglements and strong interfacial adhesion between PVA-g-GO sheets and PVA matrix. Although these high intermolecular entanglements and strong interfacial adhesion in these composite as-spun fibers were unfavorable to the orientation and crystallization of fibers during hot drawing, they were still crucial for improving the tensile strength and initial modulus of these composite drawn fibers. As shown in DMA and FTIR results (in section **3.2**), these intermolecular entanglements and interfacial adhesion between nanofillers and polymeric matrix still existed after hot drawing and heat setting. In these composite drawn fibers, these entanglements and adhesion could form a flexible interphase between polymeric matrix and nanofillers to provide a convenient path to ensure effective load transfer from PVA fiber matrix to PVA-g-GO sheets [44]. Compared polymeric

Table 4 The Mechanical properties of drawn fibers of neat PVA and PVA-g-GO/PVA composite fibers with the max draw ratio

Sample	Tensile strength (GPa)	Initial modulus (GPa)	Strain (%)
neat PVA drawn fiber	0.906 ± 0.055	15.690 ± 1.208	11.940 ± 2.076
0.13 wt% PVA-g-GO/PVA drawn fiber	1.209 ± 0.061	23.807 ± 1.174	9.227 ± 0.625
0.39 wt% PVA-g-GO/PVA drawn fiber	1.313 ± 0.085	21.244 ± 2.276	9.519 ± 0.812
0.60 wt% PVA-g-GO/PVA drawn fiber	1.257 ± 0.162	26.439 ± 3.196	8.081 ± 0.723

matrix, PVA-g-GO sheets could bear greater stress and stretch because of their higher strength and modulus. So the tensile strength and initial modulus of PVA fiber matrix could be obviously reinforced after introducing PVA-g-GO sheets.

It was worth noting that the reinforcement in tensile strength and initial modulus achieved by adding PVA-g-GO sheets was slightly lower compared to the strength and modulus achieved by adding GO directly [24]. On the one hand, DMSO as solvent was used to disperse PVA-g-GO sheets during the process of wet-spinning. Although uniform dispersion and exfoliation of PVA-g-GO sheets could be achieved in PVA matrix, the mechanical properties of PVA-g-GO/PVA composite fibers would be weakened due to the existence of plasticizer (DMSO). How to avoid the use of DMSO was one of the priorities of our future work under the premise of ensuring the uniform dispersion and exfoliation of PVA-g-GO sheets. One the other hand, the enhancement in orientation degree and crystallization degree of PVA-g-GO/PVA as-spun fibers during hot drawing was much lower than GO/PVA as-spun fibers due to the strong interfacial adhesion between PVA-g-GO sheets and PVA matrix in as-spun fibers. As for further strengthening the mechanical properties of PVA fibers, improving their orientation degree and crystallization degree was more important [24]. So how to adjust the interfacial adhesion between PVA-g-GO sheets and PVA matrix in as-spun fibers and further control the quantity of PVA chains grafted above GO sheets to maximize the orientation and crystallization of PVA-g-GO/PVA as-spun fibers under the premise of ensuring the uniform dispersion and exfoliation of PVA-g-GO sheets was also one of the priorities of our future work.

Conclusion

In conclusion, PVA-g-GO/PVA composite fibers with homogeneous dispersion and individual exfoliation of PVA-g-GO sheets could be prepared successfully via simple method of solution blending and wet spinning. Because of the PVA chains grafted above GO edges, not only the excellent dispersion and compatibility of PVA-g-GO sheets in PVA matrix could be obtained, but also these intermolecular entanglements and interfacial adhesion between PVA-g-GO sheets and PVA matrix in as-spun fibers or drawn fibers could also be enhanced. Because of these, significant reinforcement of mechanical properties of PVA-g-GO/PVA drawn fibers could be achieved. Compared with neat PVA fibers, a 39% improvement in tensile strength of composite fiber and a 69% improvement in initial modulus were obtained with the addition of 0.60 wt% of PVA-g-GO sheets. There were two factors for the obvious improvement in the mechanical property of PVA-g-GO/PVA drawn fibers. On the one hand, the crystallization degree and crystalline orientation degree of PVA-g-GO/PVA fibers could be further increased during the process of hot drawing because of the relatively weak adhesion (the template-oriented effect) between PVA-g-GO sheets and PVA matrix chains in as-spun fibers. On the other hand, the effective load transfer from PVA matrix to PVA-g-GO sheets could be achieved easily because of the relatively strong interfacial adhesion between PVA-g-GO sheets and PVA matrix chains in drawn fibers. Consequently, it was suitable and practical to prepared PVA fiber with high tensile strength and initial modulus via mechanical blending PVA-g-GO sheets into spinning solution.

Acknowledgements The financial support of Science & Technology Support Program of Sichuan Province with grant No.2016GZ0376 is gratefully acknowledged.

References

1. Baughman RH, Zakhidov AA, de Heer WA (2002) Carbon nanotubes–the route toward applications. Science 297:787–792
2. Coleman JN, Khan U, Gun'ko YK (2006) Mechanical reinforcement of polymers using carbon nanotubes. Adv Mater 18:689–706
3. Dikin DA, Stankovich S, Zimney EJ, Piner RD, Dommett GHB, Evmenenko G, Nguyen ST, Ruoff RS (2007) Preparation and characterization of graphene oxide paper. Nature 448:457–460
4. Novoselov KS, Geim AK, Morozov SV, Jiang D, Katsnelson MI, Grigorieva IV, Dubonos SV, Firsov AA (2005) Two-dimensional gas of massless Dirac fermions in graphene. Nature 438:197–200
5. Lee C, Wei XD, Kysar JW, Hone J (2008) Measurement of the elastic properties and intrinsic strength of monolayer graphene. Science 321:385–388
6. Georgantzinos SK, Giannopoulos GL, Fatsis A, Vlachakis NV (2016) Analytical expressions for electrostatics of graphene structures. Appl Surf Sci 84:27–36
7. Dong J, Yin CQ, Zhao X, Li YZ, Zhang QH (2013) High strength polyimide fibers with functionalized graphene. Polymer 54:6415–6424
8. Spinks GM, Mottaghitalab V, Bahrami-Samani M, Whitten PG, Wallace GG (2006) Carbon-nanotube-reinforced polyaniline fibers for high-strength artificial muscles. Adv Mater 18:637–640
9. Qi YY, Tai ZX, Sun DF, Chen JT, Ma HB, Yan XB, Liu B, Xue QJ (2013) Fabrication and characterization of poly(vinyl alcohol)/graphene oxide nanofibrous biocomposite scaffolds. J Appl Polym Sci 127:1885–1894
10. Zhang XF, Liu T, Sreekumar TV, Kumar S, Hu XD, Smith K (2004) Gel spinning of PVA/SWNT composite fiber. Polymer 45: 8801–8807
11. Ye HH, Lam H, Titchenal N, Gogotsi Y, Ko F (2004) Reinforcement and rupture behavior of carbon nanotubes-polymer nanofibers. Appl Phys Lett 85:1775–1777
12. Vigolo B, Pénicaud A, Coulon C, Sauder C, Pailler R, Journet C, Bernier P, Poulin P (2000) Macroscopic fibers and ribbons of oriented carbon nanotubes. Science 290:1331–1334
13. Ruan S, Gao P, Yu TX (2006) Ultra-strong gel-spun UHMWPE fibers reinforced using multiwalled carbon nanotubes. Polymer 47:1604–1611
14. Chatterjee S, Nüesch FA, Chu BTT (2013) Crystalline and tensile properties of carbon nanotube and graphene reinforced polyamide 12 fibers. Chem Phys Lett 557:92–96
15. Li JJ, Shao LS, Zhou XH, Wang YH (2014) Fabrication of high strength PVA/rGO composite fibers by gel spinning. RSC Adv 4: 43612–43618

16. Gao J, Itkis ME, Yu A, Bekyarova E, Zhao B, Haddon RC (2005) Continuous spinning of a single-walled carbon nanotube-nylon composite fiber. J Am Chem Soc 127:3847–3854
17. Yu YH, Lin CY, Yeh JM, Lin WH (2003) Preparation and properties of poly(vinyl alcohol)-clay nanocomposite materials. Polymer 44:3553–3560
18. Yang XM, Shang SM, Li L (2011) Layer-structured poly(vinyl alcohol)/graphene oxide nanocomposites with improved thermal and mechanical properties. J Appl Polym Sci 120:1355–1360
19. Arisoy B, Wu HC (2008) Material characteristics of high performance lightweight concrete reinforced with PVA. Constr Build Mater 22:635–645
20. Mu B, Li ZJ, Peng J (2000) Short fiber-reinforced cementitious extruded plates with high percentage of slag and different fibers. Cem Concr Res 30:1277–1282
21. McAllister MJ, Li JL, Adamson DH, Schniepp HC, Abdala AA, Liu J, Herrera-Alonso M, Milius DL, Car R, Prud'homme RK, Aksay IA (2007) Single sheet functionalized graphene by oxidation and thermal expansion of graphite. Chem Mater 19:4396–4404
22. Schniepp HC, Li JL, McAllister MJ, Sai H, Herrera-Alonso M, Adamson DH, Prud'homme RK, Car R, Saville DA, Aksay IA (2006) Functionalized single graphene sheets derived from splitting graphite oxide. J Phys Chem B 110:8535–8539
23. Wang B, Chen ZM, Zhang J, Cao JJ, Wang SX, Tian Q, Gao M, Xu Q (2014) Fabrication of PVA/graphene oxide/TiO2 composite nanofibers through electrospinning and interface sol-gel reaction: effect of graphene oxide on PVA nanofibers and growth of TiO2. Colloids Surf A: Physicochem Eng Asp 457:318–325
24. Zhang SC, Liu PQ, Jia EP, Zhao XS, Xu JJ, Li CL (2016) Graphene oxide reinforced poly(vinyl alcohol) composite fibers via template-oriented crystallization. J Polym Res 23:215–229
25. Zhang SC, Liu PQ, Zhao XS, Xu JJ (2017) Preparation of poly(vinyl alcohol)-grafted graphene oxide/poly(vinylalcohol) nanocomposites via in-situ low-temperature emulsion polymerization and their thermal and mechanical characterization. Appl Surf Sci 396: 1098–1107
26. Paul DG, David TG (1988) Effect of drawing on the α relaxation of poly(vinyl alcohol). J Polym Sci Part B 26:2509–2523
27. Takahiro Y, Yuji H, Di T, Daiki M, Motoyasu K, Noboru O, Junichiro K, Misao H, Hiroyasu M, Hiroki O, Yuka I, Taro M, Atsushi T (2012) Orientation of poly(vinyl alcohol) nanofiber and crystallites in non-woven electrospun nanofiber mats under uniaxial stretching. Polymer 53:4702–4708
28. Wang YJ, Tang LC, Gong LX, Yan D, Li YB, Wu LB, Jing JX, Lai GQ (2014) Grafting of epoxy chains onto graphene oxide for epoxy composites with improved mechanical and thermal properties. Carbon 69:467–480
29. Goncalves G, Marques PAAP, Barros-Timmons A, Bdkin I, Singh MK, Emami N, Gracio J (2010) Graphene oxide modified with PMMA via ATRP as a reinforcement filler. J Mater Chem 20: 9927–9934
30. Gojny FH, Schulte K (2004) Functionalisation effect on the thermomechanical behaviour of multi-wall carbon nanotube/epoxy composites. Compos Sci Technol 64:2303–2308
31. Ma PC, Mo SY, Tang BZ, Kim JK (2010) Dispersion, interfacial interaction and re-agglomeration of functionalized carbon nanotubes in epoxy composites. Carbon 48:1824–1834
32. Ajayan PM, Suhr J, Koratkar N (2006) Utilizing interfaces in carbon nanotube reinforced polymer composites for structural damping. J Mater Sci 41:7814–7819
33. Suhr J, Koratkar N (2008) Energy dissipation in carbon nanotube composites: a review. J Mater Sci 43:4370–4382
34. Potts JR, Lee SH, Alam TM, An J, Stoller MD, Piner RD, Ruoff RS (2011) Thermomechanical properties of chemically modified graphene/poly(methyl methacrylate) composites made by in situ polymerization. Carbon 49:2615–2623
35. Liang JJ, Huang Y, Zhang L, Wang Y, Ma YF, Guo TY, Chen YS (2009) Molecular-level dispersion of graphene into poly(vinyl alcohol) and effective reinforcement of their nanocomposites. Adv Funct Mater 19:2297–2302
36. Cheng HKF, Sahoo NG, Tan YP, Pan Y, Bao H, Li L, Chan SH, Zhao J (2012) Poly (vinyl alcohol) nanocomposites filled with poly (vinyl alcohol)-grafted graphene oxide. Appl Mater Interfaces 4: 2387–2394
37. Minus ML, Chae HG, Kumar S (2006) Single wall carbon nanotube templated oriented crystallization of poly (vinyl alcohol). Polymer 47:3705–3710
38. Uddin AJ, Narusawa T, Gotoh Y (2011) Enhancing mechanical properties of gel-spun poly(vinyl alcohol) fibers by iodine doping. Polym Eng Sci 51:647–653
39. Suzuki A, Murata H, Kunugi T (1998) Application of a high-tension annealing method to nylon 66 fibres. Polymer 39:1351–1355
40. Miaudet P, Badaire S, Maugey M, Derré A, Pichot V, Launois P, Poulin P, Zakri C (2005) Hot-drawing of single and multiwall carbon nanotube fibers for high toughness and alignment. Nano Letter (11):2212–2215
41. Gracía-Gutiérrez MC, Nogales A, Rueda DR, Domingo C, García-Ramos JV, Broza G, Roslaniec Z, Schulte K, Davies RJ, Ezquerra TA (2006) Templating of crystallization and shear-induced self-assembly of single-wall carbon nanotubes in a polymer-nanocomposite. Polymer 47:341–345
42. Ma JJ, Li Y, Yin X, Xu Y, Yue J, Bao JJ, Zhao T (2016) Poly(vinyl alcohol)/graphene oxide nanocomposites prepared by in situ polymerization with enhanced mechanical properties and water vapor barrier properties. RSC Adv 6:49448–49458
43. Hong PD, Miyasaka K (1994) Structure of the amorphous phase in highly drawn poly(vinyl alcohol) fibres. Polymer 35:1369–1374
44. Wang JY, Yang SY, Huang YL, Tien HW, Chin WK, Ma CCM (2011) Preparation and properties of graphene oxide/polyimide composite films with low dielectric constant and ultrahigh strength via in situ polymerization. J Mater Chem 21:13569–13575